Int. Conf. on Computational Methods for Coupled Problems in Science and Engineering
COUPLED PROBLEMS 2005
M. Papadrakakis, E. Oñate and B. Schrefler (Eds)

MODELLING OF SEMI-CONTINUOUS CASTING OF CUPRO-NICKEL ALLOYS

Frederic Pascon, Etienne Pecquet, Lihong Zhang and Anne Marie Habraken

Department of Mechanics of materials and Structures (M&S)
University of Liege
Chemin des Chevreuils 1, 4000 Liege (Belgium)
e-mail: F.Pascon@ULg.ac.be – Anne.Habraken@ULg.ac.be
web page: http://www.ulg.ac.be/matstruc

Key words: continuous casting, cupro-nickel, copper, nickel, experimental characterization, finite element method

Abstract. *This research developed at University of Liege aims to optimize the complete semi-continuous casting process at LBP Company, a producer of copper-nickel alloys (or cupro-nickels). The process consists in vertical casting of 7m long ingots. Some problems recurrently occur during casting process: formation of oscillations (wave length of about 500 mm), unsuitable concave cross-sections or internal cracks. In order to reduce the occurrence of such defects and to better understand their formation, we have been asked to develop a finite element model.*
The research focuses on two main topics: identification of material properties through laboratory tests and literature survey and the development of the numerical tool. The laboratory tests provide thermal and mechanical properties of the ingot and the mould, as well as heat transfer coefficients between the ingot and its surroundings (mould, air and water). These parameters are required for the numerical simulations of the process.
In the second part of the research, numerical calculations have been performed using finite element method. Two types of 2D models have already been studied: horizontal slice and vertical slice. This first choice has been guided by the high coupling between thermal and mechanical aspects of the problem, leading to highly complex systems of equations and subsequent long CPU times. However, due to the limitations of such 2D models, a 3D formulation has then been considered and it is still in progress.

1 INTRODUCTION

This project, entitled Lingopti and performed at the University of Liege, takes place in a First Europe research supported by the European Social Funds and the Walloon Region. The studied industrial process is a vertical semi-continuous casting of copper-nickel alloys at LBP factory in Belgium. Ingots are 7m long and their section is 930x280mm. After cooling in the mould, ingots are successively subject to air cooling, water spraying and

finally water tank cooling. LBP factory works different alloys: the main component is copper and the amount of nickel varies from a few percent to thirty percent. In some cases, iron or other components can be added. Cupro-nickels are high added values materials used in very different domains, from Euros coins to hydraulic brake tubes in automotive. The final goal of this research is the optimization of the mould and the whole casting process to improve the quality of cast products. In fact, these products sometimes present long-wave oscillations marks ($\lambda \simeq$500mm) and some ingots suffer many internal cracks. It will also be examined the influence of the content in nickel on the thermomechanical evolution of the ingot during whole the casting process.

2 LABORATORY TESTS

Laboratory tests have been carried out in several domains. In fact, cupronickel alloys are not as broadly studied as steel and even if some data are available in literature, they are not sufficient to determine thermal and mechanical properties especially at high temperatures and for the studied alloys. Experiments allow characterizing both thermal and mechanical behaviors. In addition, heat transfer coefficients have also been determined for different environment conditions.

2.1 Mechanical tests

In solidifying processes, it is essential to correctly model the material behavior from the very beginning of solidification. Hot compression tests have been carried out on cylindrical specimens (13 mm diameter by 20 mm height) at three temperatures (500, 900 and 1100°C) and three strain rates (10^{-2}, 10^{-3} and 10^{-4} s^{-1}) for CuNi 75/25 and CuNi 70/30 alloys.

Experimental stress-strain curves have then been used to fit a phenomenological model already implemented in the LAGAMINE finite element code (see numerical simulations hereafter). This model is derived from the Norton-Hoff viscoplastic law, some additional contributions being input to model stress dependency to strain and softening:

$$\overline{\sigma} = \sqrt{3} K e^{-p\overline{\varepsilon}} \left(\sqrt{3}\,\dot{\overline{\varepsilon}}\right)^m \overline{\varepsilon}^n \tag{1}$$

where $\overline{\sigma}$, $\overline{\varepsilon}$ and $\dot{\overline{\varepsilon}}$ are respectively Von Mises equivalent stress, equivalent strain and equivalent strain rate, K is consistency, m is the sensitivity to strain rate ($0 < m < 1$), n is the sensitivity to strain ($n \geq 0$) and p is the softening parameter ($p \geq 0$). All experiments have been carried out up to 70% strain. Each experiment has been performed twice if the dispersion of the results is not too large, otherwise several times. The fitted parameters are given in Table 2.1. Note that for CuNi 70/30 alloy, experimental σ–ε curves at 900°C and 1100°C and for low strain rates ($\dot{\overline{\varepsilon}} \leq 10^{-3} s^{-1}$) exhibit recrystallization.

Temperature in °C	CuNi 75/25				CuNi 70/30			
	K	m	n	p	K	m	n	p
500	412.2	0.048	0.470	0.794	467.5	0.046	0.498	0.791
900	82.56	0.166	0.110	0.135	79.92	0.147	0.098	0.000
1100	43.86	0.239	0.072	0.115	44.11	0.202	0.107	0.000

Table 1: Fitted parameters of Norton-Hoff law (consistency K in N/mm^2)

2.2 Thermal tests

The material is thermally characterized in a broad range of temperature, from 20°C to 1100°C (solidus temperature). Four parameters have been experimentally determined at ASMA Department (University of Liege):

- specific heat c_p is measured by Differential Scanning Calorimetry (DSC);
- linear thermal expansion coefficient α by dilatometry analysis;
- specific mass ρ is the ratio of the mass measured by thermogravimetry to the volume calculated by dilatometry;
- thermal diffusivity κ is measured by Laser Flash.

Then, heat conductivity k is deduced from the following relation:

$$k = \kappa \rho c_p \tag{2}$$

These parameters have been measured during heating and cooling and on columnar and equal axe zones. The variation has been found rather small, so average values have been adopted. Figure 1 summarizes the experimental results.

2.3 Heat transfer coefficients

Heat transfer is one of the most important phenomena governing the problem. This key parameter has in fact a large impact on the evolution of surface and sub-surface temperature, thus on solidification progress and development of stress and strain.

The following procedure has been developed in collaboration with IBF at RWTH University of Aachen. Specimens are bulky cylinders (40 mm diameter by 40 mm height). They are heated in a furnace up to 1150°C under inert Argon atmosphere.

Air cooling is simply measured in the lab (at room temperature – 20°C) thank to a K-type thermocouple inserted in a small hole (1.5 mm diameter) at the center of the specimen. Water spraying and water tank cooling is performed on specimens at 1150°C, 900°C, 500°C, 250°C and 100°C. The temperature of water spray is about 10°C, while water in the tank is about room temperature (20°C).

Heat transfer coefficients (h_{tc}) have been determined by finite element simulations coupled to an inverse method module called Optim, which has been developed in the

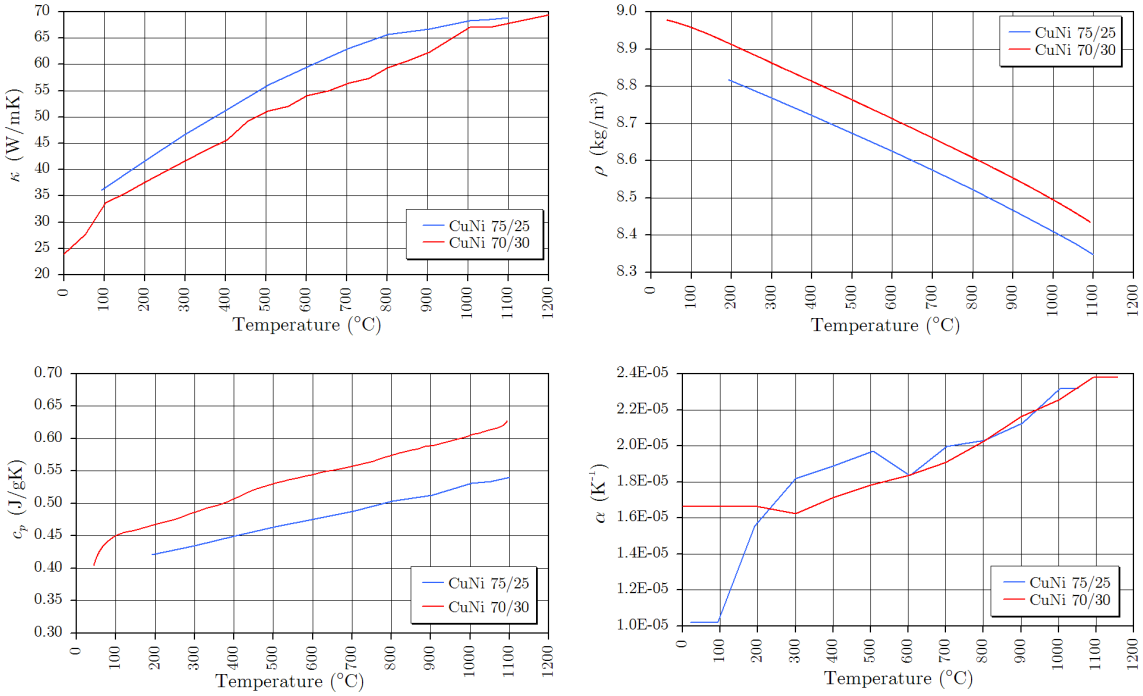

Figure 1: Thermal properties (κ, ρ, c_p and α) of both CuNi 75/25 and CuNi 70/30 alloys

M&S Department on the basis of Levenberg-Marquard algorithm [1]. Such coefficients are global values including all types of heat transfer in one coefficient: conduction, convection and radiation. h_{tc} are temperature dependent as follows:

air cooling		water spraying		water tank	
T	h_{tc}	T	h_{tc}	T	h_{tc}
400	0.02	20	2.0	20	0.2
500	0.02	100	5.0	100	2.0
750	0.08	180	4.0	180	14.0
1200	0.17	300	1.5	200	10.0
		1200	1.0	1000	3.9

Table 2: Heat transfer coefficient (in kW/m^{2}K) as a function of temperature (in °C)

Concerning cooling in the mould, it is much more complex to determine h_{tc}. Experiments have been performed on the compression test machine: in fact heat transfer is dependent on contact pressure and thus h_{tc} is pressure dependent. Specimens are flat cylinders (100 mm diameter by 30 mm height) and heated by induction. The base of the cylinder is placed on a ceramic plate considered as an adiabatic boundary limit (see Figure 2). On the top face is applied a piece of material the mould caster is made of (CuCr1Zr alloy) and another piece of steel (PM2000) the thermal properties of which

being well known.

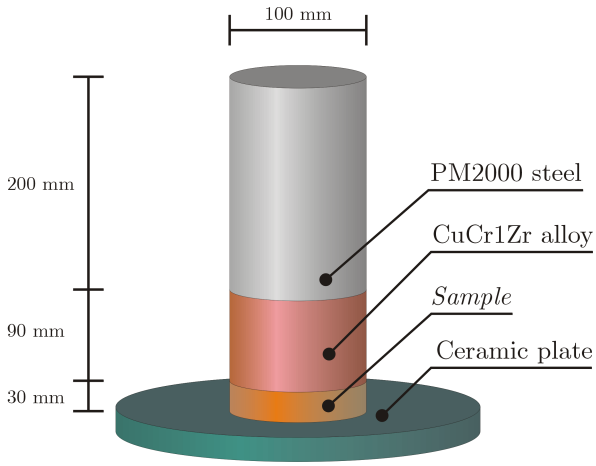

Figure 2: Experimental apparatus for determination of h_{tc} at mould interface

At the beginning of the test, the sample is at 1150°C, while the rest of the apparatus is at room temperature. The compression force is applied and temperature is monitored thanks to 5 thermocouples: 3 in the sample (at the middle and near the surface) and 2 in the CuCr1Zr alloy piece of mould. Different surface roughness have been considered: original samples exhibit circular roughness (just like the groove of a vinyl disk) due to sample machining. A second test has been performed with an old sandblasted sample (more regular surface) and a third one using the same grease as the one used in industry to lubricate the mould (the most realistic case). h_{tc} have been supposed independent on temperature, but only on pressure. The results are plotted on Figure 3. When grease is used, the contact surface is more or less independent on pressure, so that the h_{tc} is almost constant and equal to 2 kW/m^{2}K. In the two other cases, heat transfer is higher when the pressure increases. Sandblasted specimens have a higher contact surface than machined samples (roughness is lower) and they are thus favorable to higher heat transfer.

Two additional tests have been performed in lack of pressure: one with a small gap between the specimen and the "mould" piece (about a few millimeters) and a second one almost in contact. These two tests give the h_{tc} in lack of contact (as it usually happen in the corners).

3 NUMERICAL SIMULATIONS

3.1 Constitutive equations

3.1.1 Heat flow

Thermal part of the model aims to solve the transient heat flow according to initial and boundary conditions. The differential equation describing heat flow is given by:

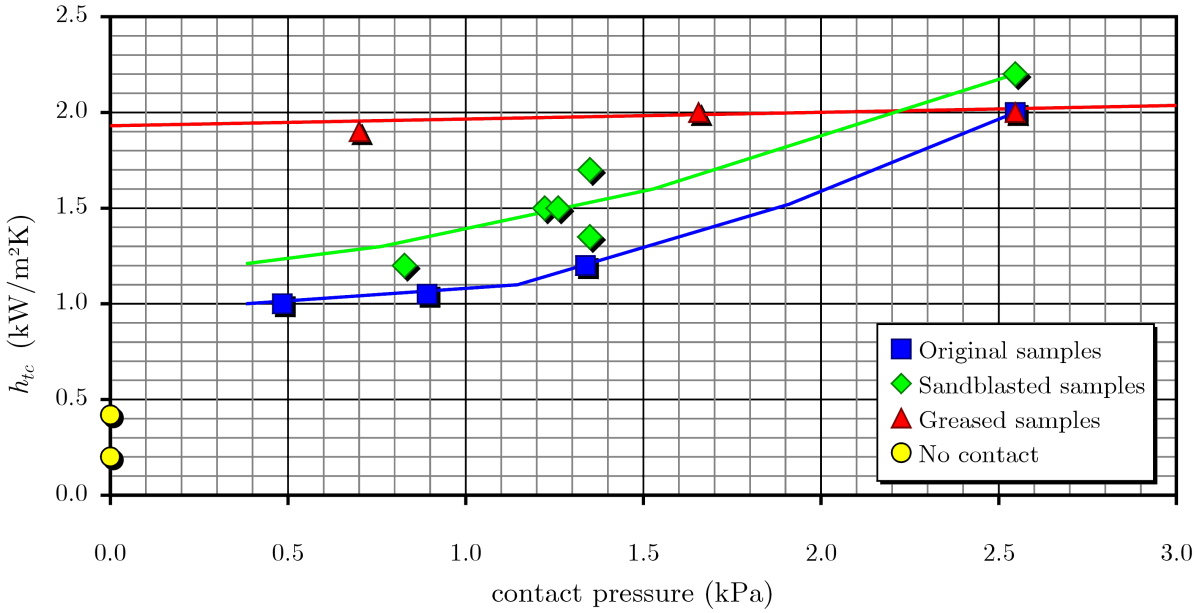

Figure 3: h_{tc} at mould interface as a function of contact pressure

$$\rho c\dot{T} + \underline{\nabla} \cdot \underline{q} = \dot{Q} \tag{3}$$

where $\dot{T}$ is the temporal derivative of temperature field, $\underline{q}$ is the heat transfer rate per unit surface (heat flux) and $\dot{Q}$ is a heat generation term, such as latent heat of solidification $\Delta\mathcal{H}_f$:

$$\dot{Q} = \rho\Delta\mathcal{H}_f \frac{\partial f_s}{\partial T}\dot{T} \tag{4}$$

In the previous expression, f_s is the solid fraction that we assume to vary linearly with respect to temperature, from zero at liquidus temperature T_{liq} to one at solidus temperature T_{sol}. Our approach is then based on the enthalpy method, which consists in defining the enthalpy function $\mathcal{H}$:

$$\mathcal{H}(T) = \int_{T_{ref}}^{T} c(\theta)\, d\theta + (1 - f_s)\Delta\mathcal{H}_f \tag{5}$$

so that the equation (3) can be written as follows:

$$\rho\dot{\mathcal{H}} + \underline{\nabla} \cdot \underline{q} = 0 \tag{6}$$

Heat transfer by conduction in the material is described by Fourier's law:

$$\underline{q} = -k\underline{\nabla}T \tag{7}$$

where $\underline{q}$ is proportional and opposite to the direction of the temperature gradient $\underline{\nabla} T$.

On the boundary of the domain, the heat flux $\underline{q}$ obeys to the Newton's law of cooling:

$$\underline{q} = h_{tc} \left(T - \overline{T}_{\infty} \right) \underline{n} \tag{8}$$

where $\overline{T}_{\infty}$ is a prescribed external temperature (mould, room or water temperature) and $\underline{n}$ is the outward normal unit vector.

3.1.2 Elastoviscoplastic mechanical law

The mechanical analysis is classically based on the separation of the total strain rate tensor $\dot{\varepsilon}_{ij}$ into mechanical and thermal contributions:

$$\dot{\varepsilon}_{ij} = \dot{\varepsilon}_{ij}^{mech} + \dot{\varepsilon}_{ij}^{th} \tag{9}$$

The apparent thermal linear expansion coefficient α is used to model volume variations due to temperature variations and solidification:

$$\dot{\varepsilon}_{ij}^{th} = \alpha \dot{T} \delta_{ij} \tag{10}$$

where δ_{ij} is the Kronecker delta.

The time integration of stress tensor σ_{ij} is based on a plasticity flow rule associated to a Von Mises' yield surface with isotropic hardening. The mechanical strain rate $\dot{\varepsilon}_{ij}^{mech}$ is composed of an elastic and a viscous-plastic parts. The elastic domain is modeled assuming a linear isotropic elastic material (Hooke's law):

$$\sigma_{ij} = \hat{\sigma}_{ij} + \sigma_m \delta_{ij} = 2G \hat{\varepsilon}_{ij}^{mech} + 3\chi \varepsilon_m^{mech} \delta_{ij} \tag{11}$$

where G is the shear modulus and χ the bulk modulus. In the above expression, $\hat{}$ symbol is used for deviatoric values and $_m$ subscript for mean values. Time integration of Hooke's law (11) takes account for variation of elastic properties during the time step:

$$\sigma_{ij,B} = \left(\frac{G_B}{G_A} \hat{\sigma}_{ij,A} + 2G_B \hat{\dot{\varepsilon}}_{ij}^{mech} \Delta t \right) + \left(\frac{\chi_B}{\chi_A} \sigma_{m,A} + 3\chi_B \dot{\varepsilon}_m^{mech} \Delta t \right) \delta_{ij} \tag{12}$$

where $_A$ and $_B$ subscripts correspond to the value of the variables at the beginning and the end of time step Δt. The viscous-plastic domain is described by a law of Norton-Hoff type, as already mentioned in section 2.1. In terms of tensors, the relation (1) becomes:

$$\hat{\dot{\varepsilon}}_{ij}^{mech} = \frac{(-J_2)^{\frac{1-m}{2m}} \, e^{\frac{p}{m}\bar{\varepsilon}} \bar{\varepsilon}^{-\frac{n}{m}}}{2 \, (K)^{\frac{1}{m}}} \hat{\sigma}_{ij} \tag{13}$$

where $J_2 = -\frac{1}{2} \hat{\sigma}_{ij} \hat{\sigma}_{ij}$ is the second invariant of deviatoric stress tensor and $\bar{\varepsilon} = \sqrt{\frac{2}{3} \dot{\varepsilon}_{ij}^{mech} \dot{\varepsilon}_{ij}^{mech}}$ the equivalent (mechanical) strain rate.

The time integration of the constitutive law is based on an implicit scheme. The stress rate tensor $\dot{\sigma}_{ij}$ can be split into deviatoric $\hat{\dot{\sigma}}_{ij}$ and mean $\dot{\sigma}_m$ parts:

$$\left\{ \begin{array}{l} \hat{\dot{\sigma}}_{ij} = 2G\left(\hat{\dot{\varepsilon}}_{ij}^{mech} - \hat{\dot{\varepsilon}}_{ij}^{vp}\right) + \frac{1}{G}\frac{\partial G}{\partial T}\hat{\sigma}_{ij}\dot{T} = f_{ij}\left(T\right) + g_{ij}\left(\hat{\sigma}_{ij}, \overline{\varepsilon}, T\right) \\ \dot{\sigma}_m = 3\chi\left(\dot{\varepsilon}_m^{mech} - \dot{\varepsilon}_m^{vp}\right) + \frac{1}{\chi}\frac{\partial \chi}{\partial T}\sigma_m\dot{T} \end{array} \right. \tag{14}$$

If $\hat{\sigma}_{ij}^A$ is the deviatoric stress tensor at the beginning A of the time step Δt, the value at the end B of the step is given by developing the relation (14) in Taylor series to the first order:

$$\begin{array}{rcl} \hat{\sigma}_{ij}^B & = & \hat{\sigma}_{ij}^A + \left(f_{ij}^A\left(T\right) + g_{ij}^A\left(\hat{\sigma}_{ij}, \overline{\varepsilon}, T\right)\right)\Delta t \\ & & + \left(\left.\frac{\partial f}{\partial T}\right|_A \theta\Delta T_{AB}\right)\Delta t + \left(\left.\frac{\partial g}{\partial \hat{\sigma}_{ij}}\right|_A \theta\Delta T_{AB}\right)\Delta t \\ & & + \left(\left.\frac{\partial g}{\partial \overline{\varepsilon}}\right|_A \theta\Delta T_{AB}\right)\Delta t + \left(\left.\frac{\partial g}{\partial T}\right|_A \theta\Delta T_{AB}\right)\Delta t \end{array} \tag{15}$$

where $0 < \theta < 1$ is a time integration parameter (equal to 2/3 in the model, according to Galerkin's time integration scheme). To simplify the expressions, the model is presented in small strain formalism, however large displacements and rotations are taken into account. The Jaumann derivatives are used to maintain objectivity.

In the same way, the time integration of mean stress σ_m is governed by:

$$\sigma_m^B = \sigma_m^A + \left(\frac{1}{\chi}\frac{\partial \chi}{\partial T}\sigma_m^A\dot{T}\right)\Delta t + 3\chi\left(\dot{\varepsilon}_m - \dot{\varepsilon}_m^{th}\right) \tag{16}$$

An additional contribution to stress tensor is due to the cuprostatic pressure p_{CuNi}. It is a hydrostatic-like pressure due to the column of liquid alloy and it is simply equal to the specific weight of molten alloy γ multiplied by the depth under the free surface D. Cuprostatic pressure is fully developed in the liquid zone and equal to zero in the solid shell. In the semi-solid area, we assumed a linear variation of p_{CuNi} with respect to liquid fraction $f_l = 1 - f_s$, so that:

$$p_{CuNi} = \gamma D\left(1 - f_s\right) = \left\{ \begin{array}{ll} \gamma D & \text{if } T_{liq} < T \\ \gamma D\left(\dfrac{T - T_{sol}}{T_{liq} - T_{sol}}\right) & \text{if } T_{sol} < T < T_{liq} \\ 0 & \text{if } T < T_{sol} \end{array} \right. \tag{17}$$

3.2 Staggered time-stepping algorithm

Casting process involves many complex phenomena and different kinds of coupling between thermal, mechanical and metallurgical aspects. Modeling such overwhelming complexity at once cannot be achieved with present computers, hence the necessity to select the key phenomena to take account for according to the expected prediction (shell behavior, solidification, fluid flow). Even if simultaneous time-stepping algorithm was

already implemented in the LAGAMINE code (as well as coupled thermo-mechanical constitutive laws [2]), a new staggered time-stepping algorithm has been used: the coupled problem is split into smaller sub-problems.

The applied time-stepping scheme is described on Figure 4. A first sub-problem governs thermal evolution and a second one the mechanical aspects. The two sub-problems are thus evolving separately with different time steps and each system of equations is easier to solve, since coupling terms between displacements and temperature evolution are not taken into account. Time scale is divided into intervals Δt_{th} compatible with the thermal problem. For each time interval Δt_{th}, the evolution of the thermal field is first computed in a thermal analysis, assuming nodes are fixed. The computed T and $\dot{T}$ are then imposed in the second sub-problem – the mechanical analysis – the nodes displacements being this time the unknowns. Then, the geometry of the thermal analysis is updated according to the previous mechanical analysis and the evolution of temperature during the second time interval Δt_{th} is computed and so on. For this application, $\Delta t_{th} = 0.25$ s.

3.3 2D approach - horizontal slice

Originally, the numerical model of continuous casting has been developed for continuous casting of steel [3, 4]. It is based on a 2.5D approach – generally known as generalized plane strain state – implemented in the finite element code LAGAMINE, which has been developed in M&S Department since early eighties. It is a non-linear large strain and displacement Lagrangian code dedicated to material forming.

The 2.5D continuous casting model is a thermoelastoviscoplastic analysis of a horizontal slice, perpendicular to the casting axis. The analysis starts just below the meniscus and it tends to model in steady-state both thermal and mechanical aspects as the slice is moving down through the caster: heat extraction, temperature distribution, solidification, stress and strain evolution in the solid shell.

The main advantage of 2D models vs. 3D is the computing time. In such non-linear complex problems, 3D simulations require very long CPU time. The first idea was therefore trying to model semi-continuous casting process using the same 2D model as for steel casting.

By gathering 2D results at each time step, corresponding to increasingly depth under free surface, it is possible to build a 3D image of the results. For example, the Figure 5 illustrates the surface temperature. Note that only one quarter of the problem is modeled, thanks to double symmetry.

It has been possible to check the model by comparing the total heat extraction rate in the mould predicted by the numerical model and the one measured in situ (deduced from the elevation in temperature of the water cooling the mould). Measurements has been estimated at 1653kW±7%, while numerical solution is about 1450kW when the heat transfer coefficient h_{tc} introduced in the equation 8 is equal to 2.0 kW/m^{2}K independently on contact pressure and progressively decreasing when the gap d is appearing according to:

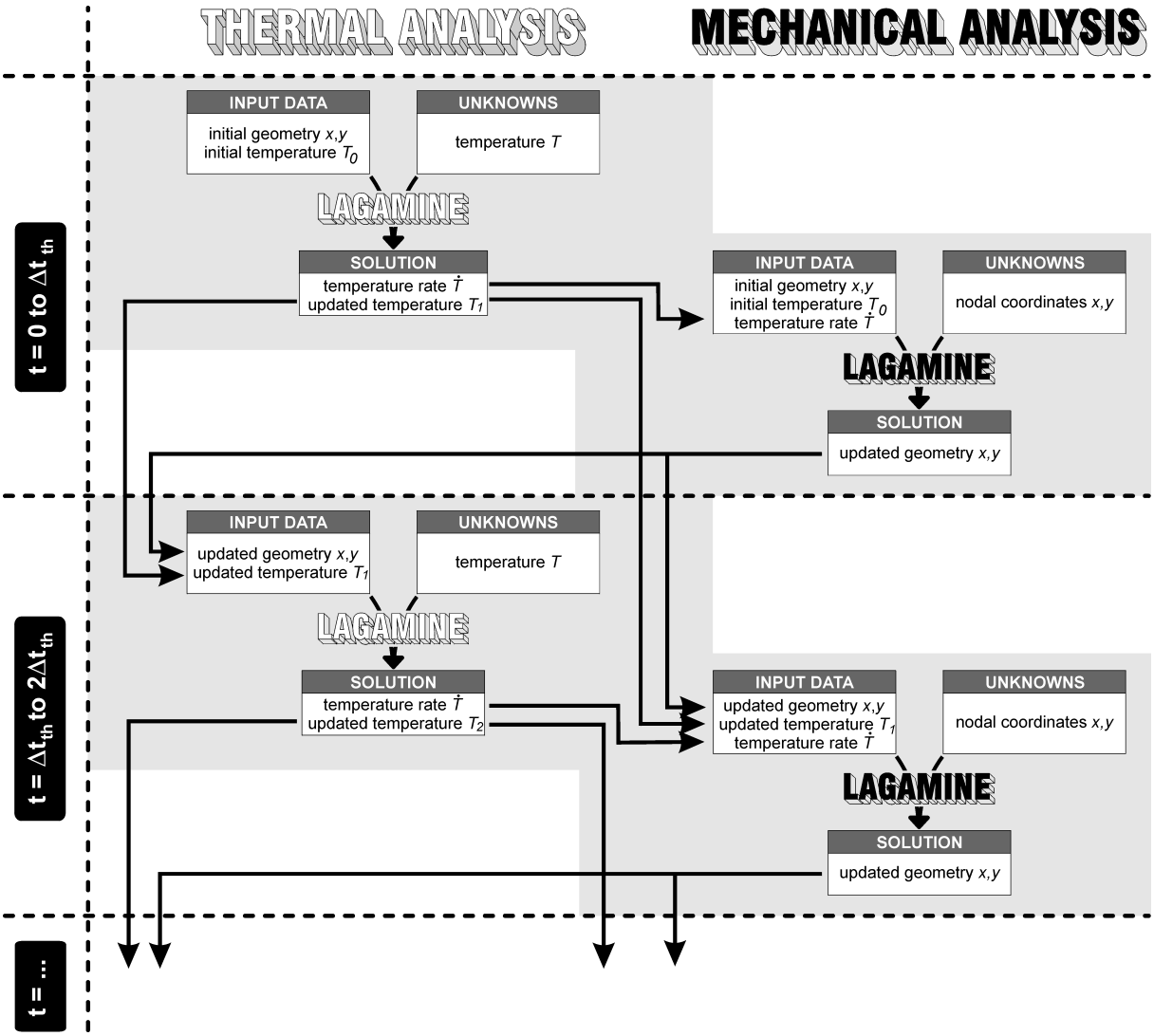

Figure 4: Staggered time-stepping algorithm

$$h_{tc}(d) = \frac{2.0\,0.15}{0.15 + 2.0\,d} \tag{18}$$

Another inspected aspect is the cross section of the ingot at the end of the process. In plant measurements gave the section illustrated on Figure 6: "barrel" distortion on the narrow faces and "pincushion" distortion on the wide faces.

Problems encountered with this model are essentially due to lack of transmission in the third direction (casting direction):

- from thermal viewpoint, no heat transfer from one slice to its neighbors;

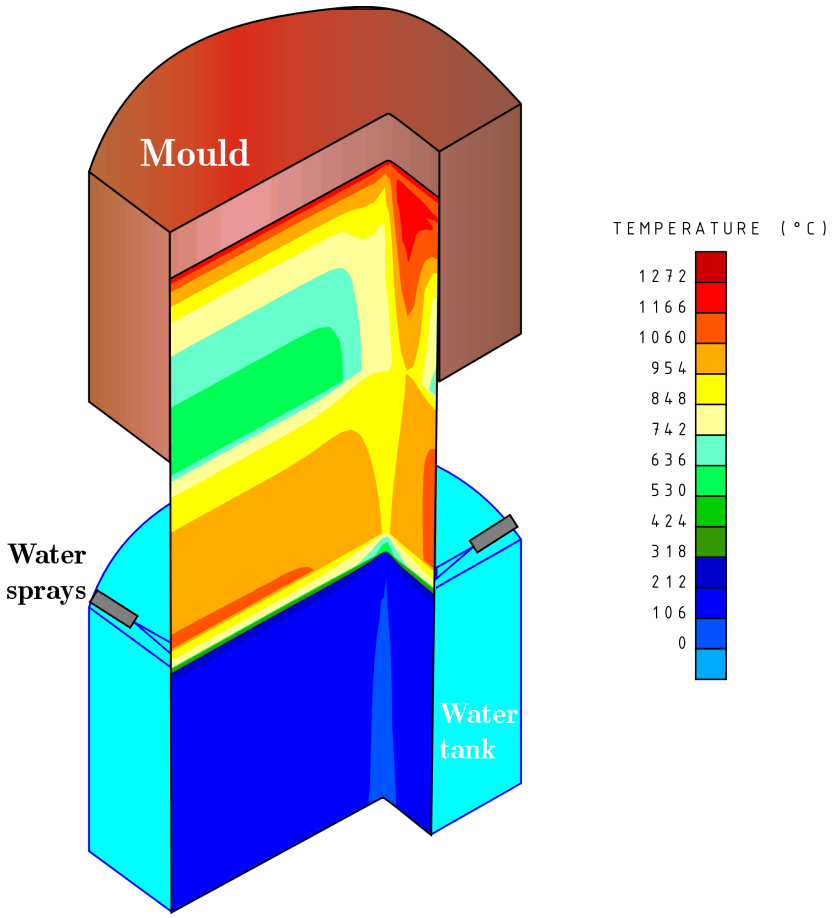

Figure 5: Surface temperature – Horizontal slice model ($\frac{1}{4}$ of the structure)

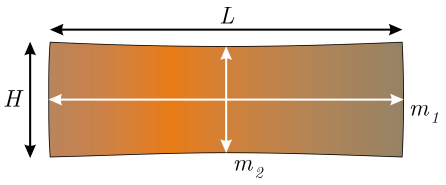

	measured	numerical
L	929 mm	938 mm
H	302 mm	303 mm
m_1	937 mm	939 mm
m_2	280 mm	326 mm (!)

Figure 6: Ingot cross section at the end of the process (as measured/computed on a CuNi 70/30 ingot)

- from mechanical viewpoint, no shear force leading to overestimated prediction of bulging (cf. m_2 value in Figure 6).

3.4 2D approach - vertical slice

The problems underlined by the horizontal slice model led us to consider a vertical slice approach, constitutive equations remaining unchanged. The slice represent the median plane of the ingot, at the middle of wide face, the symmetry of the problem allowing modeling only one half of the problem. This model underlined the vertical heat flow,

which was not taken into account in the 2D slice model, while it is not negligible, especially at low casting speed.

Since ingots are only 7m long, the beginning and the end of casting influence the evolution of the entire ingot. Therefore, the whole ingot is modeled: at the beginning, all elements are going down and ready to be taken into account, but only activated when rising the free surface level. Heat flow to the dummy bar (used to seal the mould at the beginning of filling) is also taken into account, arbitrary using 1 kW/m^{2}K as h_{tc} at this boundary and $T_{dummy} = 300$°C. In such conditions, temperature distribution is more realistic, as shown on Figure 7.

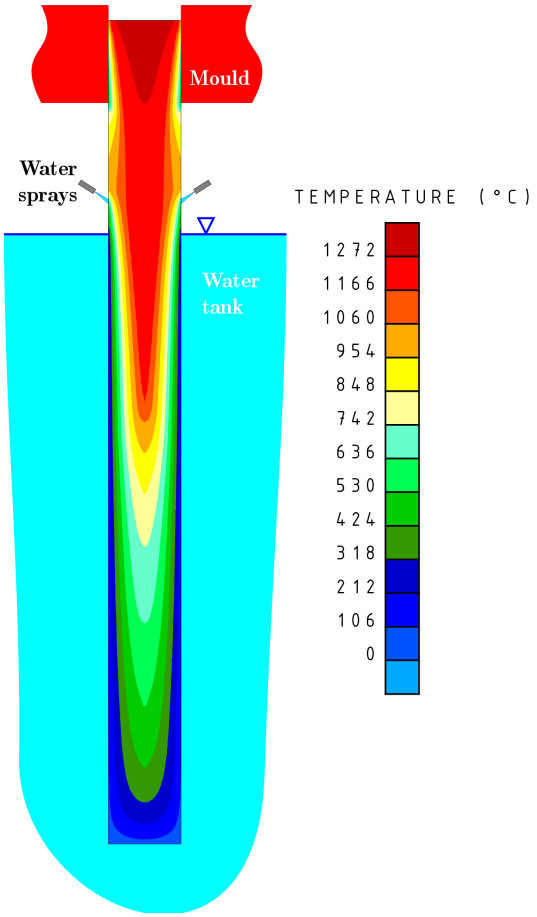

Figure 7: Temperature field with vertical slice model

Concerning the ingot distortion, the cross section is missing in such 2D vertical slice model. However, we pointed out the formation of an important air gap in the mould. In fact, the gradient of temperature in the shell thickness generates differential contraction and thus bending. Since the model is only 2D, the stiffness of the solid shell is wrong because not taking account for the complete 3D tube effect. In other respect, we clearly

see the loss of contact in the mould due to bending (cf. Figure 8).

Figure 8: Bending of the solid shell in the mould

3.5 3D approach

After having been limited by 2D models (horizontal and vertical slices), an attempt to set a 3D model is ongoing. Constitutive equations remain the same. The mesh is made of mixed-type 8-nodes hexahedral elements: an additional layer is generated and activated at each time step at the free surface while the material is going down in the caster.

Such 3D model should provide better results in terms of ingot, including the advantage of each slice models with their disadvantage: correct "tube" effect (as with horizontal slice), but also stiffness along casting direction (as the "beam" with the vertical slice). In other respects, heat flow is correctly modeled in the 3 directions.

First results have been reached with difficulties in terms of convergence and CPU time. Some problems seem to remain (especially in the mechanical calculation) and they are still under investigation. Just to give a illustration, the Figure 9 shows temperature field on the 10 first (converged) layers of the 3D model. Many convergence problems are still encountered, apparently linked to the behavior of liquid (stiffness almost equal to zero). The study is going on to solve such numerical problems by choosing appropriate assumptions on liquid part.

4 CONCLUSIONS

Two slice models have been developed to model the (semi-)continuous casting process of cupro-nickels Cu-Ni 75/25 and 70/30. Both models were helpful to get a rather quick

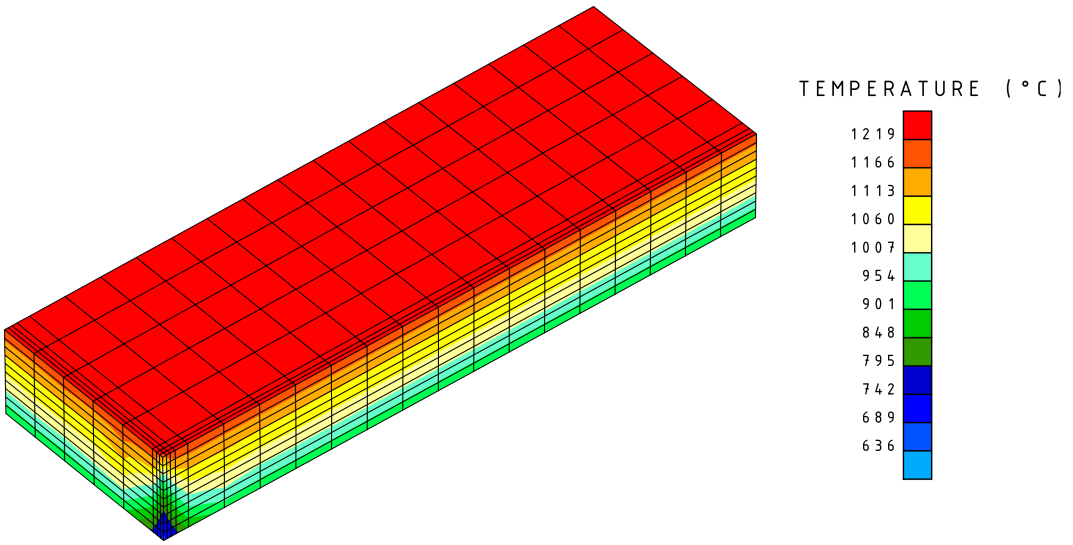

Figure 9: Temperature field on the 10 first (converged) layers of the 3D model

idea of the thermal and mechanical behavior of the material.

Experiments have been carried on to characterize the material at very high temperatures, since such data are not available in literature:

- calorimetry, dilatometry, thermogravimetry and thermal diffusivity for thermal properties;
- hot compression tests for mechanical properties;
- heat transfer coefficients under different conditions.

However both slice models exhibit limitations due to the lack of transmission of information from one slice to its two neighbors. In the case of the horizontal slice, the bulging of the slice (and thus the prediction of cross section) is completely wrong because of the lack of shear force transmission. Moreover, the heat extraction is not correctly estimated since no vertical heat transfer is taken into account. In the case of vertical slice, thermal prediction is more or less correct (for the median plane) if an approximated heat transfer coefficient is adopted in the mould. In fact, the lack of tube effect (the solidified shell), which is present in the horizontal slice model but not in the vertical one, causes the slice to badly bend and thus to lose contact with the mould.

This study thus demonstrates that, except if "equivalent" or "global" parameters are adopted, 2D models are not able to taken account for all phenomena in details. Only an approximated behavior can be modeled and it is reliant on assumptions. If a more detailed solution is expected, it is necessary to use a 3D model, much more CPU expensive, but it is the only reliable solution, especially with such good conductive materials as cupro-nickels.

REFERENCES

[1] D.S. Schnur and N. Zabaras. An Inverse Method for Determining Elastic Material Properties and a Material Interface. *Int. J. Num. Meth. Engng.* **33**, 2039–2057 (1992).

[2] A.M. Habraken and M. Bourdouxhe. Coupled thermo-mechanical-metallurgical analysis during the cooling process of steel pieces. *Eur.J.Mech.A-Solids* **11**(3), 381–402 (1992).

[3] F. Pascon. *2.5D thermal-mechanical model of continuous casting of steel using finite element method*, PhD Thesis, University of Liege (2003).

[4] S. Castagne, F. Pascon, G. Bles, A.M. Habraken. Developments in finite element simulations of continuous casting. *Journal de Physique IV* **120**, 447-455 (2004).